

Echo Technique to Distinguish Flavors of Astrophysical Neutrinos

Shirley Weishi Li,^{1,2} Mauricio Bustamante,^{1,2} and John F. Beacom^{1,2,3}

¹Center for Cosmology and AstroParticle Physics (CCAPP), Ohio State University, Columbus, OH 43210

²Department of Physics, Ohio State University, Columbus, OH 43210

³Department of Astronomy, Ohio State University, Columbus, OH 43210

li.1287@osu.edu, bustamante@osu.edu, beacom.7@osu.edu

0000-0002-2157-8982, 0000-0001-6923-0865, 0000-0002-0005-2631

(Dated: June 20, 2016)

The flavor composition of high-energy astrophysical neutrinos is a rich observable. However, present analyses cannot effectively distinguish particle showers induced by ν_e versus ν_τ . We show that this can be accomplished by measuring the intensities of the delayed, collective light emission from muon decays and neutron captures, which are, on average, greater for ν_τ than for ν_e . This new technique would significantly improve tests of the nature of astrophysical sources and of neutrino properties. We discuss the promising prospects for implementing it in IceCube and other detectors.

Introduction.— High-energy astrophysical neutrinos, long sought, were recently discovered by the IceCube Collaboration [1–6]. Their energy spectrum provides important clues about extreme astrophysical sources as well as neutrino properties at unexplored energies. However, pressing mysteries remain.

Exploiting the flavor composition — the ratios of the fluxes of $\nu_e + \bar{\nu}_e$, $\nu_\mu + \bar{\nu}_\mu$, and $\nu_\tau + \bar{\nu}_\tau$ to the total flux — offers crucial additional clues. In the nominal scenario, a composition of $(\frac{1}{3} : \frac{2}{3} : 0)_S$ at the source is transformed by neutrino vacuum mixing to $(\frac{1}{3} : \frac{1}{3} : \frac{1}{3})_\oplus$ at Earth [7, 8]. Even for arbitrary flavor composition at the source, the maximal range of flavor composition at Earth with only standard mixing is surprisingly narrow [9], making deviations sensitive indicators of new physics [10–36].

So far, IceCube measurements of the flavor composition mostly separate muon tracks — made primarily by charged-current (CC) $\nu_\mu + \bar{\nu}_\mu$ interactions — from particle showers — made by all other interactions. A significant limitation is their poor ability to distinguish between CC interactions of ν_e and ν_τ (unless noted, ν_l refers to $\nu_l + \bar{\nu}_l$).

Synopsis of the paper.— We propose a new technique to break this ν_e - ν_τ degeneracy, one that could work for a wider range of energies than existing ideas (Glashow resonance [37–39], double pulses [40], double bangs [7], and lollipops [41]).

We introduce two new shower observables. In showers, low-energy muons and neutrons are produced; after delays, the muons decay and the neutrons capture. We call the collective Cherenkov emission from the many independent decays and captures the *muon echo* and the *neutron echo*. We show that the echoes are brighter for ν_τ -initiated than for ν_e -initiated showers, which could allow them to be distinguished on a statistical basis.

Our focus is pointing out new observables to help solve the important problem of flavor identification. The technical aspects of implementation require experimental expertise. Nevertheless, in a preliminary evaluation, grounded in the measured properties of IceCube, we find the detection prospects promising.

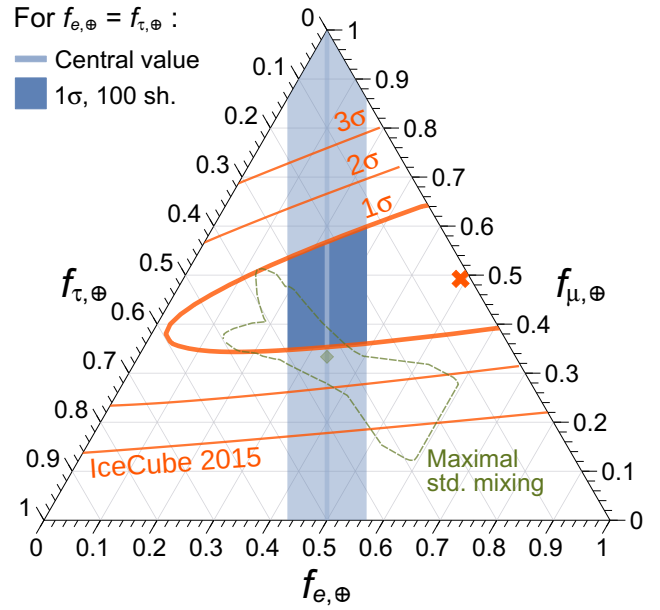


FIG. 1. Flavor composition $f_{l, \oplus}$ ($l = e, \mu, \tau$) of astrophysical neutrinos at Earth. Each axis is read parallel to its ticks. Orange: the IceCube fit [5]. Blue: the expected precision of our proposed technique (for the case $f_{e, \oplus} = f_{\tau, \oplus}$), assuming 100 showers of 100 TeV, detected with perfect efficiency (results for other energies are similar). Green: the standard expectation [7, 8] and maximal range with standard mixing [9].

Figure 1 shows that the present ν_e - ν_τ degeneracy in IceCube elongates the contours of the measured flavor composition [5]. It also shows how detecting echoes could refine these measurements, probing the flavor composition better than the maximal range with standard mixing [9], which would lead to powerful conclusions.

High-energy neutrino signatures.— At present, IceCube identifies neutrino-initiated events only as tracks and showers, for which the Cherenkov light appears to emanate from approximate lines and spheres. Tracks are caused by muons, which travel up to ~ 10 km in ice [2],

due to their low interaction and decay rates. Showers are caused by all other neutrino-induced particles and extend only ~ 10 m in ice [2], due to the high interaction and decay rates of their constituent particles.

Neutrinos produce secondaries through deep-inelastic scattering [42–44]. A neutrino interacts with a nucleon N via the CC channel $\nu_l + N \rightarrow l + X$ or the neutral-current (NC) channel $\nu_l + N \rightarrow \nu_l + X$, where $l = e, \mu, \tau$, and X represents hadrons. A fraction $(1 - y)$ of the neutrino energy goes to the final-state lepton; the remaining fraction y goes to the final-state hadrons. The inelasticity distribution peaks at $y = 0$ and has an average $\langle y \rangle \approx 0.3$ at 100 TeV, for both ν and $\bar{\nu}$, CC and NC.

Tracks are produced by ν_μ CC interactions plus 17% of ν_τ CC interactions where the tau decays to a muon [45].

Showers are produced by all other neutrino interactions. For ν_e CC interactions, the electron- and hadron-initiated showers combine, and their sum energy equals the neutrino energy. For ν_τ CC interactions, the tau decays promptly, so again the showers combine (when the tau does not decay to a muon); the neutrino energy estimate is slightly biased because $\sim 25\%$ of its energy is lost to outgoing neutrinos from tau decay. For NC interactions of all flavors, the hadron-initiated shower carries a fraction y of the neutrino energy; because of the steeply falling neutrino spectrum, NC interactions are subdominant in the total shower spectrum [46]. (This is also true for mis-identified ν_μ CC interactions that appear to be a shower event because the track is missed [31].)

These points explain the basic features of the IceCube results in Fig. 1. Because there are track events, the ν_μ component of the flux must be nonzero; because there are shower events, the sum of the ν_e and ν_τ components must be nonzero. The similarity of ν_e - and ν_τ -initiated events makes the contours nearly horizontal; the degeneracy is weakly broken because increasing the ν_τ/ν_e fraction increases the number of tracks and decreases the shower energies. With present methods, improvement requires much larger exposure [9].

Electromagnetic versus hadronic showers.—

The key to our new method is understanding the low-energy physics underlying high-energy showers [47–54].

When showers are developing, particles multiply in number while decreasing in energy. An electromagnetic shower starts out with electrons, positrons, and gamma rays and stays composed predominantly of them; there is usually a small fraction of pions and nucleons produced by photonuclear processes. A hadronic shower starts out with pions and nucleons, and then builds up a progressively larger fraction of electromagnetic particles as prompt $\pi^0 \rightarrow \gamma\gamma$ decays deplete $\sim 1/3$ of the remaining hadronic energy with each shower generation.

Shower development ends when the average particle energy is low enough that the particle- and energy-loss rates exceed the particle-production rates. At that point, the most abundant particles in all showers are ~ 100 -MeV electrons and positrons, which produce most of the prompt Cherenkov light. Pions carry only $\sim 10\%$ of the

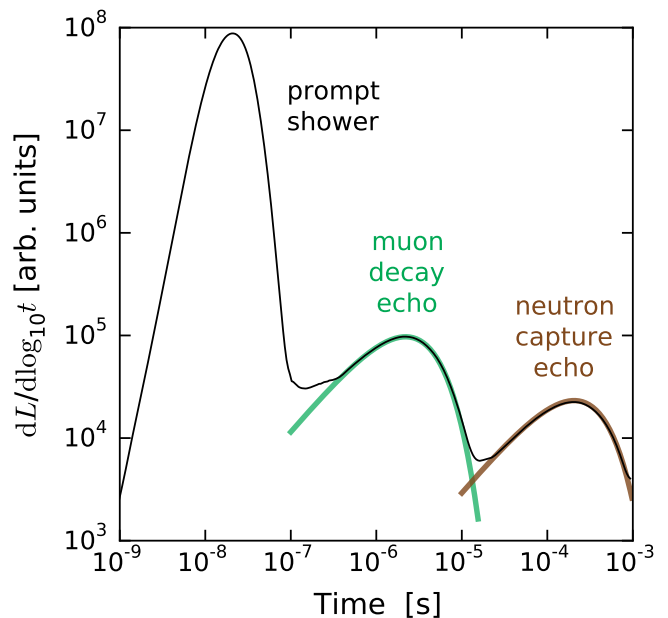


FIG. 2. Time evolution of the light yield of a hadronic shower simulated with FLUKA, following injection of a 100-TeV charged pion. The shaded bands are exponentials with the respective timescales. For an electromagnetic shower of the same prompt energy, the echoes are ~ 10 times smaller.

energy in hadronic showers and $\sim 1\%$ in electromagnetic showers. However, they are the key to separating electromagnetic and hadronic showers.

New shower observables.— At the end of shower development, charged pions come to rest by ionization; then π^- capture on nuclei and π^+ decay to μ^+ . The μ^+ decay with a lifetime of $2.2 \mu\text{s}$, producing e^+ with ~ 35 MeV. The collective Cherenkov light from these positrons is our first new observable: the *muon echo*.

Separately, neutrons lose energy by collisions until they reach thermal energy. They eventually capture on hydrogen, with a timescale of $\sim 200 \mu\text{s}$, producing 2.2 MeV gamma rays. (In seawater, 33% of neutrons capture on Cl; the emitted gamma rays have 8.6 MeV [55], making the neutron echoes more visible.) The gamma rays Compton-scatter electrons to moderate energies, producing Cherenkov light. This collective emission is our second new observable: the *neutron echo*.

We simulate showers and subsequent echoes using the FLUKA Monte Carlo software (version 2011.2c-4) [56, 57]. We inject high-energy electrons or positrons to simulate electromagnetic showers and charged pions to simulate hadronic showers.

Figure 2 shows the averaged time profile of a 100-TeV hadronic shower. Because the features happen on very different timescales, it is appropriate to analyze their light yield L in bins of log time. Accordingly, we plot $dL/d\log t \propto t dL/dt$; this makes the height of the curve proportional to its contribution to the integrated light yield. The echo shapes are exponentials with the respec-

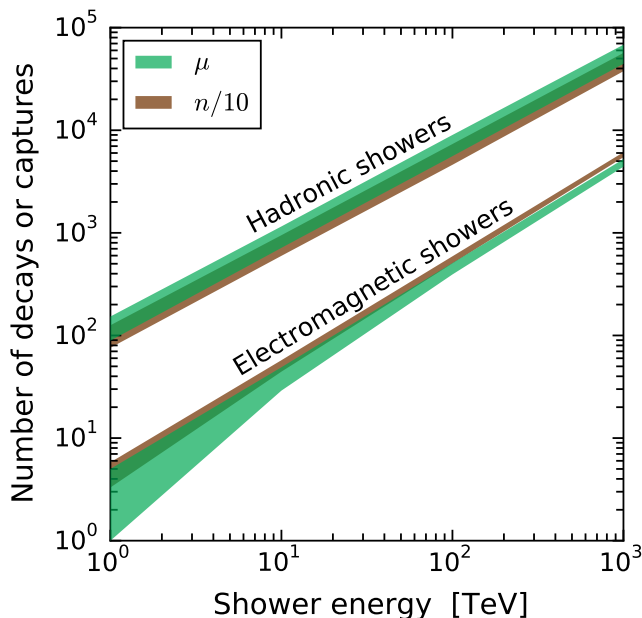


FIG. 3. Numbers of muon decays and neutron captures (scaled down by 10) per shower, as a function of shower energy, for electromagnetic and hadronic showers simulated with FLUKA. The bands show 1σ intrinsic fluctuations.

tive timescales. The echoes are well-separated from the prompt shower and from each other.

Figure 2 also shows that the echoes have low intensities: the muon echo has $\sim 3 \times 10^{-3}$ of the prompt shower energy and the neutron echo has $\sim 6 \times 10^{-4}$. The first number results from the facts that 10% of hadronic shower energy goes to pions, 10% of those pions are π^+ that come to rest and decay, and 30% of the pion decay energy goes to positrons from muon decays. The second number results from the facts that there are about 10 times more neutron captures than muon decays, that the capture energy is about 20 times smaller, and that the Cherenkov efficiency is about 3 times smaller.

The points above carry over for electromagnetic showers, except for a crucial difference: the pions carry only $\sim 1\%$ of the shower energy as opposed to $\sim 10\%$. Thus the echo intensities are expected to be ~ 10 times higher in hadronic showers than in electromagnetic showers.

Figure 3 shows that there are indeed about 10 times as many muon decays and neutron captures in hadronic showers. This difference is much larger than the intrinsic fluctuations of these numbers. Because the number of decays and captures, and, therefore, the light coming from them, grows linearly with shower energy, this factor-of-10 difference between electromagnetic and hadronic showers is present at all energies. The yields may have an overall shift of up to a factor of 2 due to hadronic and nuclear uncertainties [52, 58–60], but this can be calibrated by external measurements [61–64] or *in situ*.

Separating ν_e and ν_τ .— We now examine how echoes can be used to help identify the flavors of neutrino-

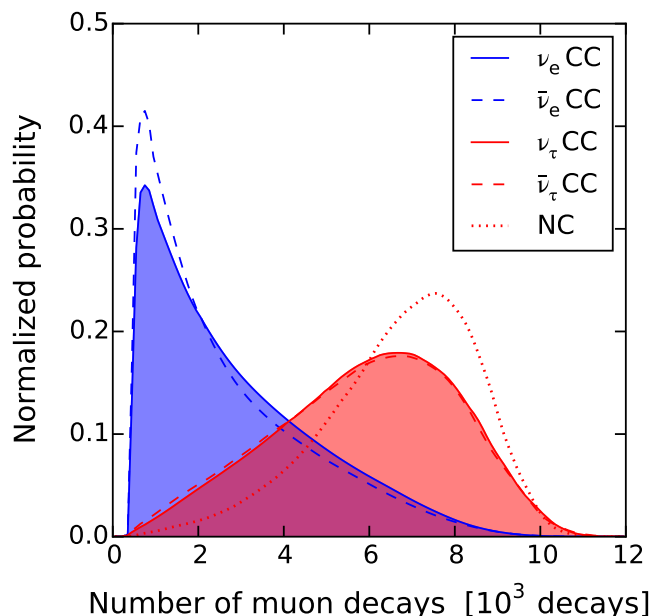


FIG. 4. Probability distributions of the numbers of muon decays per shower (of energy 100 TeV) for different neutrino interaction channels, each normalized separately.

induced showers. In realistic neutrino interactions, the differences in the echoes are less stark than above.

Showers initiated by ν_e are mostly electromagnetic because the outgoing electron typically carries more energy than the final-state hadrons. But showers initiated by ν_τ are mostly hadronic because, in addition to the shower from the final-state hadrons, 67% of tau decays are hadronic. (NC showers are purely hadronic.)

We consider flavor separation at fixed shower energy, as opposed to fixed neutrino energy, to make contact with experiment. We simulate neutrino interactions with appropriate energies to give $E_{\text{sh}} = 100$ TeV, including 10% energy resolution [65]. For NC interactions, we mimic the final-state hadrons by directly injecting charged pions at the shower energy.

Figure 4 shows how the numbers of muon decays per shower are distributed for different neutrino interaction channels. As expected, ν_e CC showers produce fewer muons than ν_τ CC showers.

The basics of the distributions in Fig. 4 can be understood easily. For pure electromagnetic showers, the peak would be at ~ 500 decays; it would be narrow because most pions are produced late in the shower and the fluctuations are mostly Poissonian. For pure hadronic showers, the peak would be at ~ 8000 decays; it would be broad because there are large fluctuations in how much energy goes into π^0 in the first few shower generations. The shapes shown in Fig. 4 depend also on the y distributions for neutrino interactions. For ν_e CC events, the distribution is substantially broadened because the differential cross section $d\sigma/dy$, while peaked at $y = 0$, has a substantial tail. For ν_τ CC events, there is a slight

shift to the left, due to the 17% of tau decays to muons.

The results in Fig. 4 make it possible to distinguish ν_e and ν_τ on a statistical basis. We next estimate the sensitivity to flavor composition using the echoes from an ensemble of events, assuming perfect detection efficiency.

First, we use the results in Fig. 4 to generate the muon decay distributions for each flavor, assuming an equal flux of ν_l and $\bar{\nu}_l$, and NC to CC event ratios consistent with a power-law spectral index of 2.5 [5]. Next, for an assumed flavor composition, we randomly sample the number of muon decays for each shower in an ensemble of 100 showers of $E_{\text{sh}} = 100$ TeV. Then, we treat the flavor composition $f_{e,\oplus}$ and $f_{\tau,\oplus}$ as free parameters ($f_{\mu,\oplus} = 1 - f_{e,\oplus} - f_{\tau,\oplus}$) and use an unbinned maximum-likelihood procedure to find their best-fit values. We generate 10^3 different realizations of the shower ensemble, and find the average best-fit values and uncertainties of $f_{e,\oplus}$ and $f_{\tau,\oplus}$. Further details are in Appendices A and B.

Figure 1 shows the predicted sensitivity on $f_{e,\oplus}$ and $f_{\tau,\oplus}$, assuming equal ν_e and ν_τ content, *i.e.*, a composition of the form $(x : 1 - 2x : x)_\oplus$, where x varies in $[0, 0.5]$. The vertical shape of the band shows that the sensitivity to $f_{e,\oplus}$ and $f_{\tau,\oplus}$ does not depend on the ν_μ content. (Because our method is only weakly sensitive to $f_{\mu,\oplus}$, we suppress its uncertainty in the plot.)

Our results are conservative. The sensitivity improves slightly with shower energy; see Appendix C. Assuming perfect detection efficiency, the sensitivity is comparable whether we use muon echoes only, neutron echoes only, or both; see Appendix D. It is also comparable, or better, for other choices of input parameters; see Appendix E.

Observability of the echoes.— Echo detection depends on how the echo light yield compares to that from ambient backgrounds and detector transients. These quantities are detector-dependent, and we use IceCube as a concrete example.

The echoes are faint, but they are well localized, which enhances their visibility. In space, like the parent shower, they are concentrated among only the few photomultiplier tubes (PMT) on a single string that are closest to the neutrino interaction vertex [66]. In time, they occur $\sim 2.2 \mu\text{s}$ and $\sim 200 \mu\text{s}$ after the prompt shower. These timescales require long-time data collection, made possible by the recent development of the HitSpooling technique, which can go to hours for infrequent events [67]. In direction, the shower light is beamed forward but the echo light is isotropic. Light scattering makes the shower more isotropic and increases its duration [65], which could partially obscure the muon echo.

The total light yield of a shower in IceCube is ~ 100 detected photoelectrons (p.e.) per TeV [2]. For 100 TeV, the muon echo in a hadronic shower is expected to yield ~ 30 p.e. and the neutron echo ~ 6 p.e. The low p.e. counts set the energy threshold for our method.

Ambient backgrounds in IceCube do not eclipse the echoes. For an average p.e. noise rate of ~ 500 Hz per PMT [68], the expected backgrounds in $2 \mu\text{s}$ and $200 \mu\text{s}$ are only $\sim 10^{-3}$ and $\sim 10^{-1}$ p.e. per PMT, respectively.

(Even with correlated noise, due to nuclear decays near the PMT, the backgrounds will be small in all but a few PMTs, and those will be identifiable [69].) And the cosmic-ray muon rate in IceCube is 3 kHz [2], so the probability of a muon lighting up several specific PMTs in the short time between shower and echo is small.

A serious concern is the detector transient called afterpulsing, where a PMT registers late p.e. with total charge proportional to the initial signal (the shower) and with a time profile characteristic to the PMT. For the IceCube PMTs, the muon echo will compete with an afterpulse feature of relative amplitude $\sim 10^{-2} E_{\text{sh}}$ near $2 \mu\text{s}$ [68]; though larger than the echo, it is not overwhelmingly so. Encouragingly, the neutron echo, though smaller, is late enough that afterpulsing seems to be negligible.

In summary, the prospects for observing echoes are promising, and they improve with shower energy. Doing so may require changes in detector design or in PMT technology [70]; these considerations may shape the design of IceCube-Gen2 [71], KM3NeT [72, 73], and Baikal-GVD [74]. With multiple nearby PMTs [71, 73, 75], it may be possible to reconstruct individual events, dramatically improving background rejection. The final word on the observability of the echoes will come from detailed studies by the experimental collaborations.

Conclusions.— The rich phenomenology contained in the flavor composition of high-energy astrophysical neutrinos cannot be fully explored due to the difficulty of distinguishing showers initiated by ν_e versus ν_τ in neutrino telescopes. To break this degeneracy, we have introduced two new observables of showers: the delayed, collective light, or “echoes,” from muon decays and neutron captures. This light reflects the size of the hadronic component of a shower, and it is stronger in ν_τ -initiated than ν_e -initiated showers.

Figure 1 shows the promise of our method for IceCube. With assumptions of 100 showers and perfect detection efficiency, echo measurements would improve the separation of ν_e and ν_τ by a factor of ~ 9 over present measurements. That is comparable to the estimated sensitivity attainable with the present technique after more than 50 years of exposure of the next-generation detector IceCube-Gen2, assuming it will have an effective area 6 times larger than IceCube.

The applications of tagging hadronic showers via muon and neutron echoes extend beyond flavor discrimination. The technique could improve shower energy reconstruction, by folding in the probability of a shower being electromagnetic or hadronic. And, at the considered energies, the echoes are shifted forward along the shower direction by ~ 5 m from the shower peak. If this shift can be detected, it would improve the poor angular resolution of showers [65].

High-energy neutrino astronomy has just begun. We are still learning the best ways to detect and analyze astrophysical neutrinos. We should pursue all potentially detectable signatures, edging closer to finding the origins and properties of these ghostly messengers.

ACKNOWLEDGMENTS

We thank Carlos Argüelles, Amy Connolly, Eric Huff, Tim Linden, Kenny Ng, David Nygren, Eric Obela, Annika Peter, Benedikt Riedel, Jakob van Santen, Shigeru Yoshida, Guanying Zhu, and especially Lutz Köpke and Anna Steuer for useful discussions and comments. We

also thank Markus Ahlers, Kfir Blum, Claudio Kopper, Carsten Rott, and others for helpful feedback beginning at JFB's presentation of these ideas at the CCAPP Cosmic Messages in Ghostly Bottles workshop in 2014. SWL, MB, and JFB are supported by NSF Grant PHY-1404311.

-
- [1] M. G. Aartsen *et al.* (IceCube Collaboration), “First observation of PeV-energy neutrinos with IceCube,” *Phys. Rev. Lett.* **111**, 021103 (2013), arXiv:1304.5356 [astro-ph.HE].
 - [2] M. G. Aartsen *et al.* (IceCube), “Evidence for High-Energy Extraterrestrial Neutrinos at the IceCube Detector,” *Science* **342**, 1242856 (2013), arXiv:1311.5238 [astro-ph.HE].
 - [3] M. G. Aartsen *et al.* (IceCube), “Search for a diffuse flux of astrophysical muon neutrinos with the IceCube 59-string configuration,” *Phys. Rev. D* **89**, 062007 (2014), arXiv:1311.7048 [astro-ph.HE].
 - [4] M. G. Aartsen *et al.* (IceCube), “Observation of High-Energy Astrophysical Neutrinos in Three Years of IceCube Data,” *Phys. Rev. Lett.* **113**, 101101 (2014), arXiv:1405.5303 [astro-ph.HE].
 - [5] M. G. Aartsen *et al.* (IceCube), “A combined maximum-likelihood analysis of the high-energy astrophysical neutrino flux measured with IceCube,” *Astrophys. J.* **809**, 98 (2015), arXiv:1507.03991 [astro-ph.HE].
 - [6] M. G. Aartsen *et al.* (IceCube), “Evidence for Astrophysical Muon Neutrinos from the Northern Sky with IceCube,” *Phys. Rev. Lett.* **115**, 081102 (2015), arXiv:1507.04005 [astro-ph.HE].
 - [7] J. G. Learned and S. Pakvasa, “Detecting tau-neutrino oscillations at PeV energies,” *Astropart. Phys.* **3**, 267–274 (1995), arXiv:hep-ph/9405296.
 - [8] H. Athar, M. Jezabek, and O. Yasuda, “Effects of neutrino mixing on high-energy cosmic neutrino flux,” *Phys. Rev. D* **62**, 103007 (2000), arXiv:hep-ph/0005104 [hep-ph].
 - [9] M. Bustamante, J. F. Beacom, and W. Winter, “Theoretically palatable flavor combinations of astrophysical neutrinos,” *Phys. Rev. Lett.* **115**, 161302 (2015), arXiv:1506.02645 [astro-ph.HE].
 - [10] J. F. Beacom, N. F. Bell, D. Hooper, S. Pakvasa, and T. J. Weiler, “Decay of high-energy astrophysical neutrinos,” *Phys. Rev. Lett.* **90**, 181301 (2003), arXiv:hep-ph/0211305 [hep-ph].
 - [11] G. Barenboim and C. Quigg, “Neutrino observatories can characterize cosmic sources and neutrino properties,” *Phys. Rev. D* **67**, 073024 (2003), arXiv:hep-ph/0301220 [hep-ph].
 - [12] J. F. Beacom, N. F. Bell, D. Hooper, S. Pakvasa, and T. J. Weiler, “Measuring flavor ratios of high-energy astrophysical neutrinos,” *Phys. Rev. D* **68**, 093005 (2003), [Erratum: *Phys. Rev. D* **72**, 019901 (2005)], arXiv:hep-ph/0307025 [hep-ph].
 - [13] J. F. Beacom, N. F. Bell, D. Hooper, S. Pakvasa, and T. J. Weiler, “Sensitivity to θ_{13} and δ in the decaying astrophysical neutrino scenario,” *Phys. Rev. D* **69**, 017303 (2004), arXiv:hep-ph/0309267 [hep-ph].
 - [14] J. F. Beacom, N. F. Bell, D. Hooper, J. G. Learned, S. Pakvasa, and T. J. Weiler, “Pseudo-Dirac neutrinos, a challenge for neutrino telescopes,” *Phys. Rev. Lett.* **92**, 011101 (2004), arXiv:hep-ph/0307151.
 - [15] Z. Z. Xing and S. Zhou, “Towards determination of the initial flavor composition of ultrahigh-energy neutrino fluxes with neutrino telescopes,” *Phys. Rev. D* **74**, 013010 (2006), arXiv:astro-ph/0603781 [astro-ph].
 - [16] P. Lipari, M. Lusignoli, and D. Meloni, “Flavor Composition and Energy Spectrum of Astrophysical Neutrinos,” *Phys. Rev. D* **75**, 123005 (2007), arXiv:0704.0718 [astro-ph].
 - [17] S. Pakvasa, W. Rodejohann, and T. J. Weiler, “Flavor Ratios of Astrophysical Neutrinos: Implications for Precision Measurements,” *JHEP* **02**, 005 (2008), arXiv:0711.4517 [hep-ph].
 - [18] A. Esmaili and Y. Farzan, “An Analysis of Cosmic Neutrinos: Flavor Composition at Source and Neutrino Mixing Parameters,” *Nucl. Phys. B* **821**, 197–214 (2009), arXiv:0905.0259 [hep-ph].
 - [19] K. C. Lai, G. L. Lin, and T. C. Liu, “Determination of the Neutrino Flavor Ratio at the Astrophysical Source,” *Phys. Rev. D* **80**, 103005 (2009), arXiv:0905.4003 [hep-ph].
 - [20] J. L. Bazo, M. Bustamante, A. M. Gago, and O. G. Miranda, “High energy astrophysical neutrino flux and modified dispersion relations,” *Int. J. Mod. Phys. A* **24**, 5819 (2009), arXiv:0907.1979 [hep-ph].
 - [21] S. Choubey and W. Rodejohann, “Flavor Composition of UHE Neutrinos at Source and at Neutrino Telescopes,” *Phys. Rev. D* **80**, 113006 (2009), arXiv:0909.1219 [hep-ph].
 - [22] M. Bustamante, A. M. Gago, and C. Pena-Garay, “Energy-independent new physics in the flavour ratios of high-energy astrophysical neutrinos,” *JHEP* **1004**, 066 (2010), arXiv:1001.4878 [hep-ph].
 - [23] M. Bustamante, A. M. Gago, and J. Jones-Perez, “SUSY Renormalization Group Effects in Ultra High Energy Neutrinos,” *JHEP* **1105**, 133 (2011), arXiv:1012.2728 [hep-ph].
 - [24] P. Baerwald, M. Bustamante, and W. Winter, “Neutrino Decays over Cosmological Distances and the Implications for Neutrino Telescopes,” *JCAP* **1210**, 020 (2012), arXiv:1208.4600 [astro-ph.CO].
 - [25] O. Mena, S. Palomares-Ruiz, and A. C. Vincent, “Flavor Composition of the High-Energy Neutrino Events in IceCube,” *Phys. Rev. Lett.* **113**, 091103 (2014), arXiv:1404.0017 [astro-ph.HE].
 - [26] K. C. Y. Ng and J. F. Beacom, “Cosmic neutrino cascades from secret neutrino interactions,” *Phys. Rev. D*

- 90, 065035 (2014), arXiv:1404.2288 [astro-ph.HE].
- [27] X. Xu, H. He, and W. Rodejohann, “Constraining Astrophysical Neutrino Flavor Composition from Leptonic Unitarity,” JCAP **1412**, 039 (2014), arXiv:1407.3736 [hep-ph].
- [28] L. Fu, C. M. Ho, and T. J. Weiler, “Aspects of the Flavor Triangle for Cosmic Neutrino Propagation,” Phys. Rev. D **91**, 053001 (2015), arXiv:1411.1174 [hep-ph].
- [29] S. Palomares-Ruiz, A. C. Vincent, and O. Mena, “Spectral analysis of the high-energy IceCube neutrinos,” Phys. Rev. D **91**, 103008 (2015), arXiv:1502.02649 [astro-ph.HE].
- [30] A. Palladino, G. Pagliaroli, F. L. Villante, and F. Vissani, “What is the Flavor of the Cosmic Neutrinos Seen by IceCube?” Phys. Rev. Lett. **114**, 171101 (2015), arXiv:1502.02923 [astro-ph.HE].
- [31] M. G. Aartsen *et al.* (IceCube), “Flavor Ratio of Astrophysical Neutrinos above 35 TeV in IceCube,” Phys. Rev. Lett. **114**, 171102 (2015), arXiv:1502.03376 [astro-ph.HE].
- [32] A. Palladino and F. Vissani, “The natural parameterization of cosmic neutrino oscillations,” Eur. Phys. J. C **75**, 433 (2015), arXiv:1504.05238 [hep-ph].
- [33] C. A. Argüelles, T. Katori, and J. Salvado, “New Physics in Astrophysical Neutrino Flavor,” Phys. Rev. Lett. **115**, 161303 (2015), arXiv:1506.02043 [hep-ph].
- [34] A. Palladino, G. Pagliaroli, F. L. Villante, and F. Vissani, “Double pulses and cascades above 2 PeV in IceCube,” Eur. Phys. J. C **76**, 52 (2016), arXiv:1510.05921 [astro-ph.HE].
- [35] I. M. Shoemaker and K. Murase, “Probing BSM Neutrino Physics with Flavor and Spectral Distortions: Prospects for Future High-Energy Neutrino Telescopes,” Phys. Rev. D **93**, 085004 (2016), arXiv:1512.07228 [astro-ph.HE].
- [36] A. C. Vincent, S. Palomares-Ruiz, and O. Mena, “Analysis of the 4-year IceCube HESE data,” (2016), arXiv:1605.01556 [astro-ph.HE].
- [37] S. L. Glashow, “Resonant Scattering of Antineutrinos,” Phys. Rev. **118**, 316 (1960).
- [38] L. A. Anchordoqui, H. Goldberg, F. Halzen, and T. J. Weiler, “Neutrinos as a diagnostic of high energy astrophysical processes,” Phys. Lett. B **621**, 18–21 (2005), arXiv:hep-ph/0410003 [hep-ph].
- [39] A. Bhattacharya, R. Gandhi, W. Rodejohann, and A. Watanabe, “The Glashow resonance at IceCube: signatures, event rates and pp vs. $p\gamma$ interactions,” JCAP **1110**, 017 (2011), arXiv:1108.3163 [astro-ph.HE].
- [40] M. G. Aartsen *et al.* (IceCube), “Search for Astrophysical Tau Neutrinos in Three Years of IceCube Data,” Phys. Rev. D **93**, 022001 (2016), arXiv:1509.06212 [astro-ph.HE].
- [41] T. DeYoung, S. Razzaque, and D. F. Cowen, “Astrophysical tau neutrino detection in kilometer-scale Cherenkov detectors via muonic tau decay,” Astropart. Phys. **27**, 238–243 (2007), arXiv:astro-ph/0608486 [astro-ph].
- [42] R. Gandhi, C. Quigg, M. H. Reno, and I. Sarcevic, “Ultrahigh-energy neutrino interactions,” Astropart. Phys. **5**, 81–110 (1996), arXiv:hep-ph/9512364 [hep-ph].
- [43] R. Gandhi, C. Quigg, M. H. Reno, and I. Sarcevic, “Neutrino interactions at ultrahigh-energies,” Phys. Rev. D **58**, 093009 (1998), arXiv:hep-ph/9807264 [hep-ph].
- [44] A. Connolly, R. S. Thorne, and D. Waters, “Calculation of High Energy Neutrino-Nucleon Cross Sections and Uncertainties Using the MSTW Parton Distribution Functions and Implications for Future Experiments,” Phys. Rev. D **83**, 113009 (2011), arXiv:1102.0691 [hep-ph].
- [45] K. A. Olive *et al.* (Particle Data Group), “Review of Particle Physics,” Chin. Phys. C **38**, 090001 (2014).
- [46] J. F. Beacom and J. Candia, “Shower power: Isolating the prompt atmospheric neutrino flux using electron neutrinos,” JCAP **0411**, 009 (2004), arXiv:hep-ph/0409046 [hep-ph].
- [47] W. Heitler, *The Quantum Theory of Radiation*, 3rd ed. (Dover Publications, 1954).
- [48] J. Matthews, “A Heitler model of extensive air showers,” Astropart. Phys. **22**, 387–397 (2005).
- [49] P. Lipari, “The Concepts of ‘Age’ and ‘Universality’ in Cosmic Ray Showers,” Phys. Rev. D **79**, 063001 (2009), arXiv:0809.0190 [astro-ph].
- [50] P. Lipari, “Universality of cosmic ray shower development,” Nucl. Phys. Proc. Suppl. **196**, 309–318 (2009).
- [51] C. Rott, J. M. Siegal-Gaskins, and J. F. Beacom, “New Sensitivity to Solar WIMP Annihilation using Low-Energy Neutrinos,” Phys. Rev. D **88**, 055005 (2013), arXiv:1208.0827 [astro-ph.HE].
- [52] S. W. Li and J. F. Beacom, “First calculation of cosmic-ray muon spallation backgrounds for MeV astrophysical neutrino signals in Super-Kamiokande,” Phys. Rev. C **89**, 045801 (2014), arXiv:1402.4687 [hep-ph].
- [53] S. W. Li and J. F. Beacom, “Spallation Backgrounds in Super-Kamiokande Are Made in Muon-Induced Showers,” Phys. Rev. D **91**, 105005 (2015), arXiv:1503.04823 [hep-ph].
- [54] S. W. Li and J. F. Beacom, “Tagging Spallation Backgrounds with Showers in Water-Cherenkov Detectors,” Phys. Rev. D **92**, 105033 (2015), arXiv:1508.05389 [physics.ins-det].
- [55] J. K. Tuli, “Evaluated Nuclear Structure Data File (ENSDF),” <http://www.nndc.bnl.gov/ensdf/>, [Online; accessed 2016-05-20].
- [56] A. Ferrari, P. R. Sala, A. Fasso, and J. Ranft, “FLUKA: A multi-particle transport code (Program version 2005),” (2005).
- [57] G. Battistoni *et al.*, “The FLUKA code: Description and benchmarking,” AIP Conf. Proc. **896**, 31–49 (2007).
- [58] S. Abe *et al.* (KamLAND), “Production of Radioactive Isotopes through Cosmic Muon Spallation in KamLAND,” Phys. Rev. C **81**, 025807 (2010), arXiv:0907.0066 [hep-ex].
- [59] G. Bellini *et al.* (Borexino), “Cosmogenic Backgrounds in Borexino at 3800 m water-equivalent depth,” JCAP **1308**, 049 (2013), arXiv:1304.7381 [physics.ins-det].
- [60] Y. Zhang *et al.* (Super-Kamiokande), “First measurement of radioactive isotope production through cosmic-ray muon spallation in Super-Kamiokande IV,” Phys. Rev. D **93**, 012004 (2016), arXiv:1509.08168 [hep-ex].
- [61] J. F. Beacom and M. R. Vagins, “GADZOOKS! Antineutrino spectroscopy with large water Cherenkov detectors,” Phys. Rev. Lett. **93**, 171101 (2004), arXiv:hep-ph/0309300 [hep-ph].
- [62] M. Askins *et al.* (WATCHMAN), “The Physics and Nuclear Nonproliferation Goals of WATCHMAN: A Water Cherenkov Monitor for Antineutrinos,” (2015), arXiv:1502.01132 [physics.ins-det].
- [63] I. Anghel *et al.* (ANNIE), “Letter of Intent: The Accelerator Neutrino Neutron Interaction Experiment (AN-

- NIE),” (2015), arXiv:1504.01480 [physics.ins-det].
- [64] P. Fernandez (Super-Kamiokande), “Status of GAD-ZOOKS!: Neutron Tagging in Super-Kamiokande,” *Proceedings, 37th International Conference on High Energy Physics (ICHEP 2014)*, Nucl. Part. Phys. Proc. **273-275**, 353–360 (2016).
 - [65] M. G. Aartsen *et al.* (IceCube), “Energy Reconstruction Methods in the IceCube Neutrino Telescope,” JINST **9**, P03009 (2014), arXiv:1311.4767 [physics.ins-det].
 - [66] C. Kopper, “Recent IceCube Results on High Energy Neutrinos,” http://macros2013.in2p3.fr/_shared/doc/talks/kopper.pdf, MACROS 2013.
 - [67] M. G. Aartsen *et al.* (IceCube), “The IceCube Neutrino Observatory Part V: Neutrino Oscillations and Supernova Searches,” (2013), arXiv:1309.7008 [astro-ph.HE].
 - [68] R. Abbasi *et al.* (IceCube), “Calibration and Characterization of the IceCube Photomultiplier Tube,” Nucl. Instrum. Meth. A **618**, 139–152 (2010), arXiv:1002.2442 [astro-ph.IM].
 - [69] M. J. Larson, *Simulation and Identification of Non-Poissonian Noise Triggers in the IceCube Neutrino Detector*, Master’s thesis, The University of Alabama (2013).
 - [70] M. P. Bristow, “Suppression of afterpulsing in photomultipliers by gating the photocathode,” Appl. Opt. **41**, 4975–4987 (2002).
 - [71] M. G. Aartsen *et al.* (IceCube), “IceCube-Gen2: A Vision for the Future of Neutrino Astronomy in Antarctica,” (2014), arXiv:1412.5106 [astro-ph.HE].
 - [72] U. F. Katz, “KM3NeT: Towards a km³ Mediterranean Neutrino Telescope,” Nucl. Instrum. Meth. A **567**, 457–461 (2006), arXiv:astro-ph/0606068 [astro-ph].
 - [73] S. Adrian-Martinez *et al.* (KM3Net), “Letter of Intent for KM3NeT2.0,” (2016), arXiv:1601.07459 [astro-ph.IM].
 - [74] A. V. Avrorin *et al.*, “Current status of the BAIKAL-GVD project,” Nucl. Instrum. Meth. A **725**, 23–26 (2013).
 - [75] E. Resconi, “The stepping stones to proton decay: IceCube, PINGU, MICA,” https://indico.cern.ch/event/224351/contributions/466197/attachments/368604/513012/Aspen_2013_Resconi.pdf, Aspen Center for Physics, New Directions in Neutrino Physics 2013.
 - [76] R. Laha, J. F. Beacom, B. Dasgupta, S. Horiuchi, and K. Murase, “Demystifying the PeV Cascades in IceCube: Less (Energy) is More (Events),” Phys. Rev. D **88**, 043009 (2013), arXiv:1306.2309 [astro-ph.HE].

Supplemental Material

In the main text, we showed how detecting muon echoes can improve discrimination between ν_e -initiated and ν_τ -initiated showers. We showed results using 100-TeV showers and a flavor composition of the form $(x : 1 - 2x : x)_\oplus$. Here we provide more details on the statistical method and show how the results depend on choices of inputs.

In Appendix A, we present the underlying formalism for flavor discrimination per shower. In Appendix B, we apply it to an ensemble of showers. In Appendix C, we discuss flavor discrimination at other shower energies. In Appendix D, we discuss neutron echoes. In Appendix E, we show sensitivity results for other input choices.

To simplify the notation, we explicitly show the shower energy E_{sh} dependence when defining a quantity, and suppress it otherwise. In the probability definitions, we show ν CC cases explicitly; NC and $\bar{\nu}$ cases have similar definitions, with CC replaced by NC, and ν replaced by $\bar{\nu}$.

Appendix A: Flavor discrimination for one shower

We calculate the probability that an observed shower, containing N_μ muon decays, was initiated by a neutrino ν_l , of definite flavor $l = e, \mu$, or τ .

The main observable of a shower is its energy E_{sh} , which is proportional to the total collected light. Because the detector energy resolution is narrow, we simply take it to be flat in the range $[0.9, 1.1] E_{\text{sh}}$.

Using Bayes' theorem, the probability that a shower with energy E_{sh} and N_μ muon decays was initiated by a ν_l is

$$P_{\nu_l|N_\mu}(E_{\text{sh}}) = \frac{P_{N_\mu|\nu_l}^{\text{CC}} P_{\nu_l}^{\text{CC}} + P_{N_\mu|\nu_l}^{\text{NC}} P_{\nu_l}^{\text{NC}}}{\sum_{\alpha=e,\mu,\tau} \left[\left(P_{N_\mu|\nu_\alpha}^{\text{CC}} P_{\nu_\alpha}^{\text{CC}} + P_{N_\mu|\bar{\nu}_\alpha}^{\text{CC}} P_{\bar{\nu}_\alpha}^{\text{CC}} \right) + \left(P_{N_\mu|\nu_\alpha}^{\text{NC}} P_{\nu_\alpha}^{\text{NC}} + P_{N_\mu|\bar{\nu}_\alpha}^{\text{NC}} P_{\bar{\nu}_\alpha}^{\text{NC}} \right) \right]}. \quad (\text{A1})$$

Here, $P_{\nu_l}^{\text{CC}}(E_{\text{sh}})$ is the probability that a shower with energy E_{sh} is produced by the CC interaction of a ν_l , which we detail below, while $P_{N_\mu|\nu_l}^{\text{CC}}(E_{\text{sh}})$ is the probability that said shower yields N_μ muon decays, which is calculated via FLUKA simulations and shown in Figs. 4 and A3 for different shower energies.

The probability $P_{\nu_l}^{\text{CC}}$ is defined as

$$P_{\nu_l}^{\text{CC}}(E_{\text{sh}}) = \frac{N_{\nu_l}^{\text{CC}}}{\sum_{\alpha=e,\mu,\tau} (N_{\nu_\alpha}^{\text{CC}} + N_{\bar{\nu}_\alpha}^{\text{CC}}) + (N_{\nu_\alpha}^{\text{NC}} + N_{\bar{\nu}_\alpha}^{\text{NC}})}, \quad (\text{A2})$$

where $N_{\nu_l}^{\text{CC}}(E_{\text{sh}})$ is the number of ν_l -initiated showers generated by CC interactions. The denominator in Eq. (A2) is the total number of showers initiated by all flavors of neutrinos and anti-neutrinos.

To calculate the number of showers, we use the “theorist’s approach” [76], assuming perfect detector efficiency at the relevant energies. The final results on flavor discrimination are affected by only the relative, not the absolute, event rates from different flavors. We consider a flux F_{ν_l} of ν_l (in units of $\text{GeV}^{-1} \text{cm}^{-2} \text{s}^{-1} \text{sr}^{-1}$) arriving at the detector, which contains \mathcal{N} target nucleons. The flux already includes any attenuation due to propagation in the Earth. In observation time Δt with detection solid angle $\Delta\Omega$, the number of detected ν_l -initiated CC showers is

$$N_{\nu_l}^{\text{CC}}(E_{\text{sh}}) = \mathcal{N} \cdot \Delta t \cdot \Delta\Omega \cdot \int_0^\infty F_{\nu_l}(E_\nu) \cdot \sigma_\nu^{\text{CC}}(E_\nu) \cdot g_{\nu_l}^{\text{CC}}(E_\nu, E_{\text{sh}}) dE_\nu, \quad (\text{A3})$$

where E_ν is the neutrino energy and σ_ν^{CC} is the neutrino-nucleon CC cross section [42–44]. The function $g_{\nu_l}^{\text{CC}}$ is the probability that a neutrino with energy E_ν creates a shower with energy E_{sh} ; it is different for each flavor.

- In ν_e CC interactions, all of the neutrino energy is deposited in the electromagnetic and hadronic showers. Accordingly, we define

$$g_{\nu_e}^{\text{CC}} = \begin{cases} 1, & \text{if } E_\nu \in [0.9, 1.1] E_{\text{sh}} \\ 0, & \text{otherwise} \end{cases}. \quad (\text{A4})$$

- In ν_τ CC interactions, the outgoing tau has numerous decay modes. All of them have outgoing neutrinos, which carry away energy and do not appear in the shower, so that $E_{\text{sh}} \lesssim E_\nu$. On average, the outgoing neutrinos carry away 40% of the tau energy, or 25% of the primary neutrino energy. For simplicity, we make $g_{\nu_\tau}^{\text{CC}}$ nonzero only in the energy range $E_\nu \in [0.9, 1.1] E_{\text{sh}}/0.75$. Since 17% of tau decays are into muons and neutrinos, without a shower, we estimate

$$g_{\nu_\tau}^{\text{CC}} = \begin{cases} 0.83, & \text{if } E_\nu \in [0.9, 1.1] E_{\text{sh}}/0.75 \\ 0, & \text{otherwise} \end{cases}. \quad (\text{A5})$$

- In NC interactions, the energy deposited in the shower is the energy of the final-state hadrons, *i.e.*, $E_{\text{sh}} = yE_\nu$. For the shower energy to lie within 10% of E_{sh} , the value of y must lie in the range $[y_{\text{min}}, y_{\text{max}}] \equiv [0.9, 1.1]E_{\text{sh}}/E_\nu$. Hence, we define

$$g_{\nu_l}^{\text{NC}}(E_\nu) = \frac{\int_{y_{\text{min}}}^{y_{\text{max}}} \frac{d\sigma_\nu^{\text{NC}}}{dy}(E_\nu, y) dy}{\int_0^1 \frac{d\sigma_\nu^{\text{NC}}}{dy}(E_\nu, y) dy}, \quad (\text{A6})$$

where $d\sigma_\nu^{\text{NC}}/dy$ is the y probability distribution for NC interactions [44]. However, because hadron-initiated showers carry a small fraction y of the neutrino energy, and because the neutrino flux is steeply falling, NC showers are subdominant to CC showers [46].

- In ν_μ CC interactions, the outgoing muon leaves an identifiable track. We exclude these events by setting

$$g_{\nu_\mu}^{\text{CC}} = 0. \quad (\text{A7})$$

We have assumed that no track is mis-identified as a shower; otherwise, the value of $g_{\nu_\mu}^{\text{CC}}$ would be set to the probability of mis-identification. As with NC events, these would be subdominant in the shower spectrum.

We write Eqs. (A1)–(A3) in a more useful way. Consider an all-flavor astrophysical neutrino flux $\propto E_\nu^{-\gamma}$ and flavor ratios at Earth ($f_{e,\oplus} : f_{\mu,\oplus} : f_{\tau,\oplus}$), such that the flux of ν_l is $F_{\nu_l} = f_{l,\oplus} F_0 E_\nu^{-\gamma}$, with F_0 the normalization of the flux. With this, Eq. (A3) becomes

$$N_{\nu_l}^{\text{CC}}(E_{\text{sh}}) = \mathcal{N} \cdot \Delta t \cdot \Delta\Omega \cdot F_0 \cdot f_{l,\oplus} \cdot I_{\nu_l}^{\text{CC}}(E_{\text{sh}}), \quad (\text{A8})$$

with the shorthand

$$I_{\nu_l}^{\text{CC}}(E_{\text{sh}}) \equiv \int_0^\infty E_\nu^{-\gamma} \cdot \sigma_\nu^{\text{CC}}(E_\nu) \cdot g_{\nu_l}^{\text{CC}}(E_\nu, E_{\text{sh}}) dE_\nu. \quad (\text{A9})$$

Finally, using Eqs. (A8) and (A9), and assuming equal flavor ratios for neutrinos and anti-neutrinos, Eq. (A1) becomes

$$P_{\nu_l|N_\mu}(E_{\text{sh}}) = \frac{f_{l,\oplus} \left[P_{N_\mu|\nu_l}^{\text{CC}} I_{\nu_l}^{\text{CC}} + P_{N_\mu|\nu_l}^{\text{NC}} I_{\nu_l}^{\text{NC}} \right]}{\sum_{\alpha=e,\mu,\tau} f_{\alpha,\oplus} \left[\left(P_{N_\mu|\nu_\alpha}^{\text{CC}} I_{\nu_\alpha}^{\text{CC}} + P_{N_\mu|\bar{\nu}_\alpha}^{\text{CC}} I_{\bar{\nu}_\alpha}^{\text{CC}} \right) + \left(P_{N_\mu|\nu_\alpha}^{\text{NC}} I_{\nu_\alpha}^{\text{NC}} + P_{N_\mu|\bar{\nu}_\alpha}^{\text{NC}} I_{\bar{\nu}_\alpha}^{\text{NC}} \right) \right]}. \quad (\text{A10})$$

The probability that the shower with N_μ muon decays was created by a ν_l or a $\bar{\nu}_l$ is simply $P_{\nu_l|N_\mu} + P_{\bar{\nu}_l|N_\mu}$.

Figure A1 shows this probability computed at $E_{\text{sh}} = 100$ TeV, assuming a diffuse astrophysical neutrino flux with spectral index $\gamma = 2.5$ and a flavor composition of $(\frac{1}{3} : \frac{1}{3} : \frac{1}{3})_\oplus$, compatible with IceCube results [5]. The neutrino is more likely to be a ν_e if there are fewer muon decays and a ν_τ if there are more decays. The probability that the shower is from a ν_μ NC interaction (not shown) reaches at most 10%, at large values of N_μ .

Appendix B: Flavor discrimination for an ensemble of showers

We use the results from Appendix A to infer the $f_{e,\oplus}$ and $f_{\tau,\oplus}$ flavor ratios of an ensemble of showers. We first explain how we generate the artificial shower ensemble; then we show how to infer their flavor ratios.

To generate an ensemble of showers with energy E_{sh} , we first assume a neutrino flux with spectral index $\gamma = 2.5$ and “real” values for the flavor ratios ($f_{e,\oplus}^r : f_{\mu,\oplus}^r : f_{\tau,\oplus}^r$). We then use the probability distribution functions of the number of muon decays for each channel, $P_{N_\mu|\nu_l}^{\text{CC}}$ and $P_{N_\mu|\nu_l}^{\text{NC}}$ (shown in Figs. 4 and A3), to construct the total probability distribution of muon decays associated to that flux, by summing over all flavors and interaction channels:

$$P_{\mu,\text{tot}}(N_\mu; E_{\text{sh}}, \{f_{l,\oplus}^r\}) = \sum_{\alpha=e,\mu,\tau} \left[P_{N_\mu|\nu_\alpha}^{\text{CC}} \cdot P_{\nu_\alpha}^{\text{CC}}(f_{\alpha,\oplus}^r) + P_{N_\mu|\nu_\alpha}^{\text{NC}} \cdot P_{\nu_\alpha}^{\text{NC}}(f_{\alpha,\oplus}^r) \right] + [\nu_\alpha \rightarrow \bar{\nu}_\alpha].$$

Figure A2 shows the total muon decay distribution for $E_{\text{sh}} = 100$ TeV, for three choices of flavor composition. The distribution for our nominal case $(\frac{1}{3} : \frac{1}{3} : \frac{1}{3})_\oplus$ has a saddle shape, peaked at low number of decays due to the sharp distribution of the ν_e CC channel. The height of this peak increases with $f_{e,\oplus}^r$.

We use the above distribution to randomly sample the number of muon decays for each shower, that is, we obtain $N_{\mu,i}$ for $i = 1, \dots, N_{\text{sh}}$. These are our “real” data. We choose $N_{\text{sh}} = 100$, consistent with near-future expectations for IceCube.

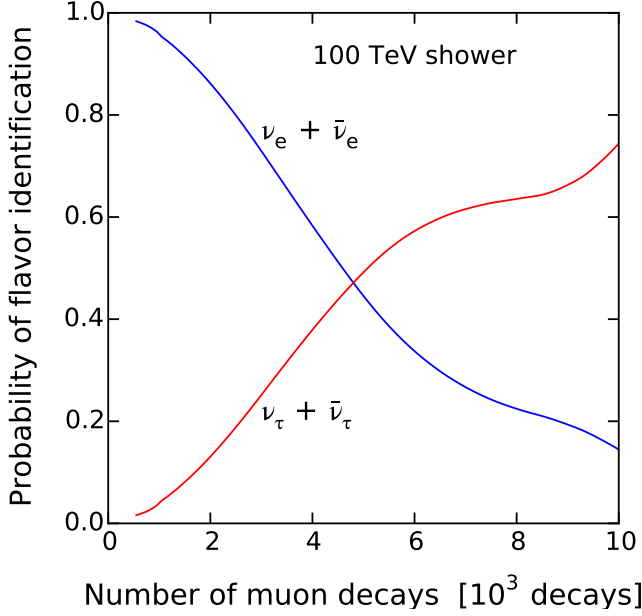


FIG. A1. Probability that one neutrino-induced shower was generated by a ν_e (via either CC or NC) or ν_τ , as a function of number of muon decays. The curve for ν_μ is calculated but not shown.

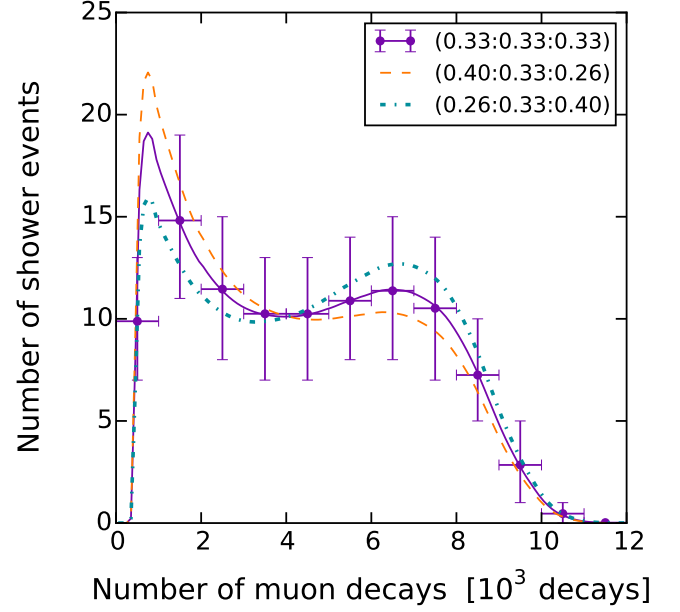


FIG. A2. Distributions of muon decays for an ensemble of 100 showers of 100 TeV, for different choices of flavor composition ($f_{e,\oplus} : f_{\mu,\oplus} : f_{\tau,\oplus}$), reflecting the central value and width of the band in Fig. 1.

Merely to illustrate the flavor separation power given this sample size, we include binned data for this choice in Fig. A2. The points and error bars show the expected number of showers per bin and its 1σ Poissonian fluctuation. The power of flavor discrimination using muon echoes hinges on the ratio of the number of showers with few muon decays — *e.g.*, $N_\mu < 3000$ — to the number of showers with many muon decays — *e.g.*, $N_\mu > 6000$. A higher ratio drives $f_{e,\oplus}$ up and $f_{\tau,\oplus}$ down, and vice versa.

For our actual analysis, we recover the flavor ratios $f_{l,\oplus}^r$ of the ensemble via an unbinned maximum likelihood approach. The likelihood function for a test flavor composition ($f_{e,\oplus} : f_{\mu,\oplus} : f_{\tau,\oplus}$), with $f_{\mu,\oplus} \equiv 1 - f_{e,\oplus} - f_{\tau,\oplus}$, is

$$\mathcal{L}(f_{e,\oplus}, f_{\tau,\oplus}) = G(f_{\mu,\oplus}) \prod_{i=1}^{N_{\text{sh}}} P_{\mu,\text{tot}}(N_{\mu,i}; f_{e,\oplus}, f_{\tau,\oplus}) . \quad (\text{B1})$$

The Gaussian term, $G(f_{\mu,\oplus})$, constrains the muon component from deviating too much from its true value, assuming it can be measured from a separate track analysis. We choose the 1σ width of the Gaussian to be 0.12, consistent with the present IceCube measurement [5].

The maximum value of the likelihood determines the best-fit values of $f_{e,\oplus}$, $f_{\tau,\oplus}$, and $f_{\mu,\oplus} = 1 - f_{e,\oplus} - f_{\tau,\oplus}$. To estimate the uncertainty on this value, we repeat the maximum likelihood procedure using 1000 random realizations of the real data. Figure 1 shows the best-fit values and uncertainties on $f_{e,\oplus}$ and $f_{\tau,\oplus}$ that result from this procedure, assuming ensembles of $N_{\text{sh}} = 100$ showers each and real flavor ratios $f_{e,\oplus}^r = f_{\tau,\oplus}^r = (1 - f_{\mu,\oplus}^r)/2$, with $f_{\mu,\oplus}^r$ varying in the range $[0, 1]$.

Appendix C: Results for different energies

In the main text, we consider showers of 100 TeV; the normalized distribution of number of muon decays for this shower energy is shown in Fig. 4.

Figure A3 shows the distributions at 10 TeV and 1 PeV. The same general shapes and behavior of the curves is seen at all energies: ν_e -initiated CC showers have appreciably fewer muon decays than ν_τ -initiated CC showers and NC showers. The main change is in the intensity of the muon echo, which scales roughly linearly with shower energy.

As the shower energy changes, there are moderate changes in the results. The value of $\langle y \rangle$ decreases with increasing energy, which means that ν_e -initiated CC showers become more leptonic. And the y distributions for ν and $\bar{\nu}$ become

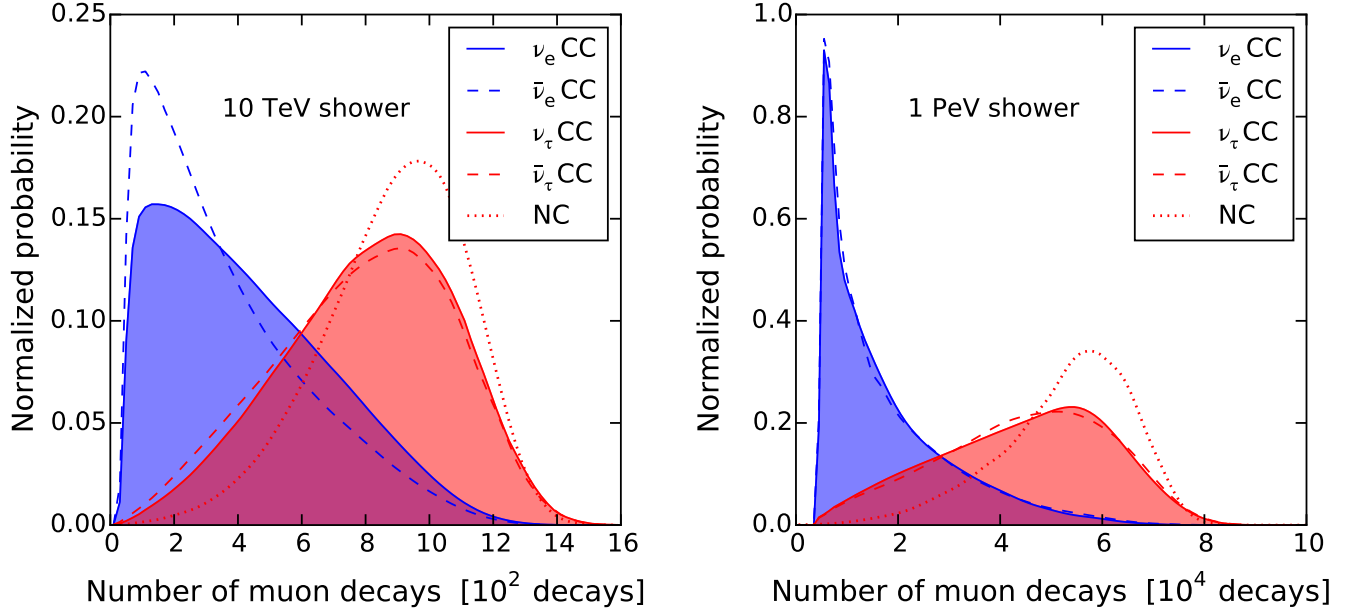


FIG. A3. Normalized distributions of the numbers of muon decays per shower of energy 10 TeV and 1 PeV for different neutrino interaction channels. Note the changes in x -axis scale compared to Fig. 4.

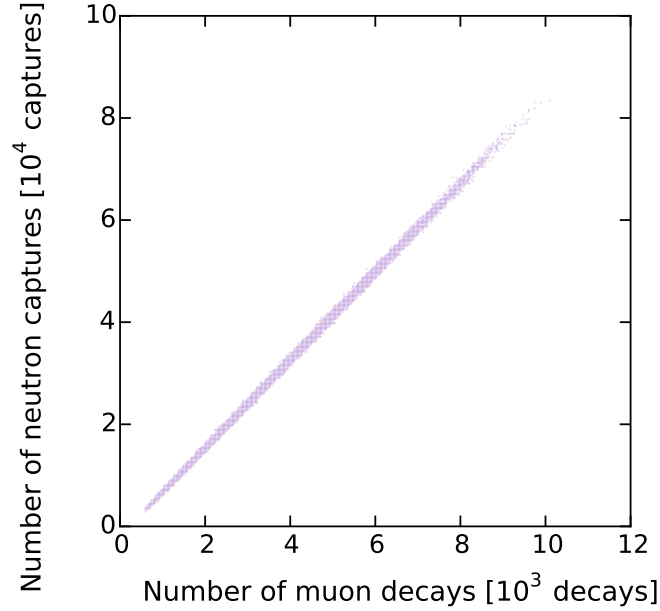


FIG. A4. Correlations between numbers of muon decays and neutron captures for individual 100 TeV ν_e CC shower. Note the different axis scales.

more similar at higher energies, and, therefore, so do their muon decay distributions. Therefore, the separation between ν_e and ν_τ becomes cleaner at higher energies. This is evidenced by contrasting the panels in Fig. A3.

Appendix D: Results for neutron echoes

Like the muon echo, the neutron echo is a product of the hadronic component of a shower.

Figure A4 shows that the number of muon decays and the number of neutron captures is tightly correlated on an event-by-event basis. Because of this, the probability distributions of the numbers of neutron captures behave

similarly to those of muon decays (Figs. 4 and A3), except for a scaling of the x -axis by a factor of about 10.

If we were to incorporate neutron echoes in our sensitivity estimate, Eq. (B1) would have an extra term $\prod_{i=1}^{N_{\text{sh}}} P_{n,\text{tot}}(N_{n,i}; f_{e,\oplus}, f_{\tau,\oplus})$ on the right-hand side, with $N_{n,i}$ the number of neutron captures in each shower of the ensemble. However, the distribution of number of neutron captures, $P_{n,\text{tot}}$, is essentially just $P_{\mu,\text{tot}}$ scaled up by a factor of 10. Therefore, adding it to the likelihood would not alter the best-fit values of $f_{e,\oplus}$ and $f_{\tau,\oplus}$ or their uncertainties.

This is true from a theoretical perspective. However, from an experimental perspective, neutron echoes are attractive because there seems to be less PMT afterpulsing at late times.

Finally, there is a third possible post-shower signal — the spallation echo — coming from the collective Cherenkov light from beta decays of long-lived (~ 0.1 – 10 s) unstable nuclei. These isotopes, which are a background in low-energy neutrino detectors, are produced more efficiently in hadronic than electromagnetic showers, by a factor ~ 10 [52–54]. While the spallation echo is not observable in IceCube or similar detectors due to ambient backgrounds, it might have an application in another context.

Appendix E: Results for other input choices

Figure A5 shows the flavor sensitivity, using muon echoes, for three different assumptions of the flavor composition at Earth, including the one shown in Fig. 1.

For the choice of flavor composition in Fig. 1, the average 1σ uncertainty was 0.07. For $(0 : 2x : 1 - 2x)_{\oplus}$, with $x \in [0, 0.5]$, the best-fit values lie on the left axis of the plot; only the one-sided 1σ range, of size 0.01, is visible. For $(1 - 2x : 2x : 0)_{\oplus}$, the best-fit values lie on the right axis of the plot; the one-sided 1σ range, of size 0.04, is visible. These are two extreme choices. Their smaller uncertainties are due to the fact that the total distribution of muon decays of the shower ensemble is dominated by the distribution from either ν_e -initiated or ν_{τ} -initiated CC showers. Hence, our nominal choice of flavor composition, in Fig. 1, was conservative, as it has the largest uncertainty.

At fixed shower energy, the uncertainty on the ν_e fraction scales as $\sqrt{N_{\text{sh}}}$, subject to some caveats. When N_{sh} is small ($\lesssim 20$), the likelihood is basically flat, and one typically cannot break the ν_e - ν_{τ} degeneracy with good precision. When N_{sh} is large ($\gtrsim 1000$), one should take a narrower prior on the ν_{μ} fraction to reflect its measurement being correspondingly better.

The flavor sensitivity is robust against other input choices. For example, the average 1σ uncertainty is virtually unaffected for a harder neutrino flux of $\gamma = 2$, compared to $\gamma = 2.5$.

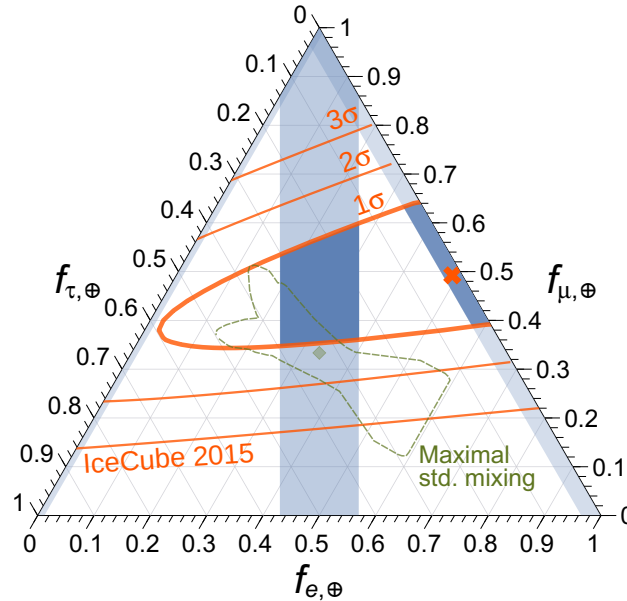


FIG. A5. Expected precision of our proposed technique for 100 detected showers at 100 TeV, for different assumptions of the flavor composition $f_{l,\oplus}$ ($l = e, \mu, \tau$) of astrophysical neutrinos at Earth: $(0 : 2x : 1 - 2x)_{\oplus}$ (left band), $(x : 1 - 2x : x)_{\oplus}$ (central band, same as in Fig. 1), and $(1 - 2x : 2x : 0)_{\oplus}$ (right band), with $x \in [0, 0.5]$.